Characterization of the Inherent Resilience of Large Cities to Natural Hazards

Nicos Makris, F.ASCE[1]; Tue Vu, M.ASCE[2]; Gholamreza Moghimi, S.M.ASCE[3]; Georgios Chatzikyriakidis, S.M.ASCE[4]; and Eric Godat[5]

Abstract: In view that cities will continue to house the majority of the world's population at an increasing rate in the face of climate change, this paper studies urban resilience by examining the response history of the mean-square displacement of the citizens of large cities prior to and upon historic natural hazards strike. The recorded mean-square displacements of large numbers of cellphone users from the cities of Houston, Miami, and Jacksonville when struck by hurricanes Harvey 2017, Irma 2017, and Dorian 2019 together with the recorded mean-square displacements of the citizens of Dallas and Houston when experiencing the 2021 North American winter storm suggest that large cities of average population density when struck by natural hazards are inherently resilient. The recorded mean-square displacements presented in this study also validate a mechanical model for cities, previously developed by the authors, that is rooted in Langevin dynamics and predicts that following a natural hazard, large cities revert immediately to their initial steady-state behavior and resume their normal, preevent activities. The inherent ability of large American cities to revert to their normal, preevent, steady-state response as evidenced in this study by the recorded mean-square displacement of their citizens needs to be further explored for other cities around the world with different resources, and socioeconomic structures. **DOI: 10.1061/JENMDT.EMENG-7102.**

Introduction

Natural hazards such as earthquakes, hurricanes, coastal flooding, winter storms, and wildfires, among others, are environmental phenomena that have the potential to impact the infrastructure of societies together with their urban and natural environment (Smith and Katz 2013). In view that cities will continue to house the majority of the world's population at an increasing rate in association with the face of climate change; urban resilience is an increasingly popular subject among scholars and policymakers (Bruneau et al. 2003; Godschalk 2003; Cimellaro et al. 2010; Da Silva et al. 2012; Jabareen 2013; Meerow et al. 2016).

Urbanization is an ever-growing, pressing challenge. As recently as 1950, only 30% of the world's population lived in cities. Today more than 50% is urbanized, and by 2,050, more than ¾ of the world's population is expected to live in cities (Brockerhoff 1998; Bettencourt and West 2010). As cities continue to grow, many of them along the coasts of continents that are prone to natural hazards, urban resilience has become a subject of interest in various disciplines (Bruneau et al. 2003; Godschalk 2003; Da Silva et al. 2012; Jabareen 2013; Meerow et al. 2016). The many challenges associated with rapid urban growth, community resilience, and sustainable development are receiving increasing attention; yet, in practice, they have been treated as independent issues (Bettencourt and Kaur 2011).

Our definition of *urban resilience* adopted in this study is rooted in the seminal work of Holling (1973, 1996), who distinguishes *engineering resilience* from *ecological resilience*. The more traditional definition associated with *engineering resilience* hinges upon the ability of a system to *assume stable equilibrium* (or steady-state regime at equilibrium), and in this case, resilience is defined as the capacity of the system, following a disturbance (shock), to recover its initial equilibrium state and revert to its normal, preevent activity. The second definition associated with *ecological resilience* emphasizes conditions *far from equilibrium* where instabilities can flip a system into another regime of behavior—that is, a different equilibrium state. In this case, resilience is associated with the magnitude of a disturbance (shock) that needs to be absorbed by the system before it changes its structure and stabilizes at a different equilibrium state (Holling 1996). In this work, which builds upon our past study (Makris et al. 2023), *urban resilience to natural hazards* is defined as the ability of a large city, following a natural hazard, to revert to its initial steady-state behavior and resume its normal, preevent activities—a definition that matches Holling's (1996) definition of engineering resilience.

Cities are complex networks or even networks of complex networks (Gao et al. 2012)–including the transportation infrastructure (roads, bus lines, and a subway network when available), water and gas utility networks, the electricity grid, telecommunication networks (telephone and internet) together with overriding social networks (Bettencourt 2013; Lhomme et al. 2013; Cruz et al. 2013). Fig. 1 shows schematically the superposition of the various aforementioned infrastructure networks for the Dallas metroplex in Texas. All these complex networks have been created and upgraded independently at different times with no apparent common design principles. In addition to these aforementioned material, electricity, and electronic networks, perhaps the most robust network that

[1]Professor, Dept. of Civil and Environmental Engineering, Southern Methodist Univ., Dallas, TX 75275 (corresponding author). ORCID: https://orcid.org/0000-0002-9059-2147. Email: nmakris@smu.edu

[2]Research Scientist, Data Science and Research Services, Office of Information Technology (OIT), Southern Methodist Univ., Dallas, TX 75275.

[3]Postdoctoral Fellow, Dept. of Civil and Environmental Engineering, Southern Methodist Univ., Dallas, TX 75275. ORCID: https://orcid.org/0000-0001-5950-5204

[4]Ph.D. Student, Dept. of Civil and Environmental Engineering, Southern Methodist Univ., Dallas, TX 75275.

[5]Team Lead, Data Science and Research Services, Office of Information Technology (OIT), Southern Methodist Univ., Dallas, TX 75275. ORCID: https://orcid.org/0000-0002-1484-199X

Note. This manuscript was submitted on December 2, 2022; approved on May 22, 2023; published online on July 28, 2023. Discussion period open until December 28, 2023; separate discussions must be submitted for individual papers. This paper is part of the ***Journal of Engineering Mechanics***, © ASCE, ISSN 0733-9399.

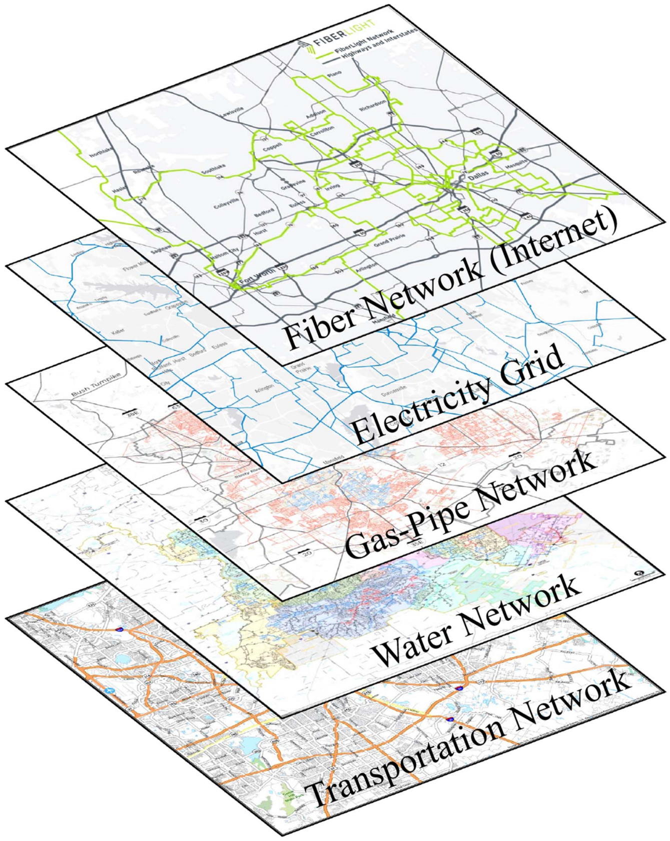

Fig. 1. Transportation, utility, and telecommunication infrastructure networks of the Dallas metroplex that have been created and upgraded independently during different times with no apparent common design principles. The superposition of these independent infrastructure networks creates a difficult-to-interpret "redundancy" that apparently serves urban resilience.

serves urban resilience is the living network of the citizens since cities are essentially the physical manifestation of the daily interactions of its citizens facilitating the generation of creativity, growth, progress, and leadership together with economic, intellectual, and social wealth.

While the functionality of cities is served with the superposition of a variety of large-scale, complex networks as schematically shown in Fig. 1 with no apparent common design principles, it appears that cities display a difficult-to-interpret self-organizing behavior that leads to deterministic patterns. In an effort to express mathematically this emergent, self-organizing behavior in association with the need to develop a quantitative, science-based understanding of the dynamics and response of cities when subjected to natural hazards, Makris et al. (2023) envisioned a city to be a matrix where people (cellphone users) are driven by the city's economy and other personal and societal driving incentives while using the collection of its infrastructure networks similarly as thermally driven Brownian particles move within a complex viscoelastic material (Mason and Weitz 1995; Mason et al. 1997a, b; Gittes et al. 1997; Schnurr et al. 1997; Mason 2000; Huang et al. 2011; Jannasch et al. 2011; Li and Raizen 2013).

Mobile phones carried by the citizens of a large city offer rich data on human mobility patterns, and we show that ensemble averages of cellphone GPS location data [mean-square displacement (MSD)] reveal detailed information on the response of cities to natural hazards as well as to sudden evacuation orders. Our study concentrates on a "*single-state equilibrium*" which is the *response history of the mean-square displacement* of the citizens of the entire city when it operates under normal conditions–a response parameter that describes with remarkable fidelity the physical manifestation of the daily interactions of the citizens of a large city through their collective mobility patterns. Our study examines: (1) the recorded mean-square displacement $= \langle r^2(t) \rangle$ from three large US cities (Houston, Miami, and Jacksonville) when subjected to category 4 and 5 hurricanes (2017 Harvey, 2017 Irma, and 2019 Dorian), and (2) the response of the Dallas and Houston metroplexes that were subjected to the February 2021 North American winter storm; and reveals that the MSD $= \langle r^2(t) \rangle$ of all the aforementioned cities when subjected to the corresponding violent natural hazard reverts immediately to its preevent pattern upon the expiration of the duration of the natural hazard. This invariant, systematic ability of large American cities following a natural hazard to revert immediately to their initial steady-state behavior and resume their normal, preevent activities suggests that large American cities are inherently resilient to natural hazards. The analysis presented in this paper is system wide for the entire urban center. The response and recovery time of smaller, local communities in these large American cities to natural hazards will be examined in a future study together with the response of other cities around the world with different resources and socioeconomic structures.

Brownian Motion and Langevin Dynamics

Brownian motion is the thermally driven random motion of microparticles (Brownian particles such as pollen grains, organelles, or macromolecules having a size from submicrometer to a few micrometers) immersed in a fluid due to the random forces, $f_R(t)$, that originate from the random collisions of the rapidly moving fluid molecules on the Brownian particles (Landau and Lifshitz 1980; Attard 2012). Since Einstein's (1905) seminal paper that presented for the first time the long-term relation (diffusive regime) between the mean-square displacement of Brownian particles, $r^2(t)$, and the diffusion coefficient of the fluid, D ($\langle r^2(t) \rangle = 2Dt$), there has been a growing interest on this physical process given that the equation that describes the motion of a Brownian particle immersed in some liquid that is in thermal equilibrium applies to a wide range of stochastic (random) processes from which deterministic time-response functions emerge when the system is at a steady-state equilibrium (Mason and Weitz 1995; Attard 2012; Li and Raizen 2013; Coffey and Kalmykov 2012).

Soon after Einstein's (1905) paper in which Brownian motion was explained by solving a diffusion equation, Langevin (1908) explained Brownian motion by adopting an entirely different approach (Landau and Lifshitz 1980; Attard 2012; Coffey and Kalmykov 2012). In his 1908 seminal paper, Langevin mingles statistical and continuum mechanics to formulate the equation of motion of a Brownian microsphere with radius R, and mass m, suspended in a Newtonian viscous fluid with viscosity, η, when subjected to the random forces, $f_R(t)$, that originate from the collisions of the fluid molecules (of the order of 10^{14} collisions per second) on the Brownian microsphere

$$m\frac{d\boldsymbol{v}(t)}{dt} = -\zeta\boldsymbol{v}(t) + f_R(t) \tag{1}$$

where $\boldsymbol{v}(t) = d\boldsymbol{r}(t)/dt$ = particle velocity and $\zeta\boldsymbol{v}(t)$ is a viscous drag force which according to Stoke's law; and $\zeta = 6\pi R\eta$ (Landau and Lifshitz 1959). The random excitation, $f_R(t)$, has a zero-average value over time, $\langle f_R(t) = 0 \rangle$, while for the memoryless, Newtonian viscous fluid that only dissipates energy, the correlation function contracts to a Dirac delta function (Lighthill 1958)

$$\langle f_R(t_1) f_R(t_2) \rangle = A\delta(t_1 - t_2) \tag{2}$$

with A = constant that expresses the strength of the random force.

Given the random nature of the excitation force $f_R(t)$, the Langevin Eq. (1) can be integrated in terms of ensemble averages in association with Eq. (2). The mean-square displacement of particles suspended in a viscous fluid with viscosity, η, was first evaluated by Ornstein (1917) (see also Uhlenbeck and Ornstein 1930) for all time scales (including the ballistic regime at early times)

$$\langle r^2(t) \rangle = \frac{NK_B T}{3\pi R} \frac{1}{\eta} (t - \tau(1 - e^{-t/\tau})) \tag{3}$$

where $N \in \{1, 2, 3\}$ = number of spatial dimensions; K_B = Boltzmann's constant; T = equilibrium temperature of the fluid; and $\tau = m/(6\pi R\eta)$ = dissipation time of the perpetual fluctuation-dissipation process that governs Brownian motion.

In a recent paper, Makris (2020) showed that the time-response function $\frac{1}{\eta}(t - \tau(1 - e^{-t/\tau}))$ appearing on the right-hand side of Eq. (3) is the creep compliance (strain history due to a unit-step stress) of the inertoviscous fluid (Makris 2017, 2018) that is a parallel connection of a dashpot with viscosity η (the viscosity of the Newtonian fluid within which the Brownian particles are immersed) and an inerter with distributed inertance, $m_R = m/(6\pi R)$ with units $[M][L]^{-1}$

$$J(t) = \frac{1}{\eta} (t - \tau(1 - e^{-t/\tau})) \tag{4}$$

Accordingly, Eq. (3) can be expressed as

$$\langle r^2(t) \rangle = \frac{NK_B T}{3\pi R} J(t) \tag{5}$$

The result of Eq. (5) is of central interest in this work because it relates the mean-square displacement—that is an ensemble average from a stochastic (random) process, to a deterministic time-response function that is the creep compliance (strain history due to a unit-step stress) of the inertoviscous fluid. Building on the work of Mason and Weitz (1995) in association with the work of Wang and Uhlenbeck (1945), Makris (2020) showed that Eq. (5) is invariably true for Brownian motion within any linear, isotropic viscoelastic fluid where $J(t)$ is the creep compliance (retardation function) of a viscoelastic network that is a parallel connection of the linear viscoelastic material within which the Brownian particles are immersed and an inerter with distributed inertance $m_R = m/(6\pi R)$. Eq. (5) also holds for the case where the density of the fluid surrounding the Brownian microparticles is appreciable (Makris 2021b); and in this case, in addition to the Stokes viscous drag, the Brownian motion of the immersed microparticles develops the Boussinesq hydrodynamic memory (Boussinesq 1885).

A Mechanical Model for Cities

In view of the overarching validity of Eq. (5) regardless of the complexity of the mechanism that the immersed Brownian particles exchange forces with the surrounding fluid (viscous, inertia, hydrodynamic memory, or viscoelastic forces), Makris et al. (2023) built upon the profound implications of Eq. (5) to conjecture a corresponding relation for cities

$$\langle r^2(t) \rangle = WJ(t) = A_0 \left\{ U(t-0) - C\left[\cos(\omega_R t) + \frac{\gamma}{2}\left(\sin\left(\frac{8}{7}\omega_R t\right) - \sin\left(\frac{6}{7}\omega_R t\right) \right) \right] \right\} \tag{6}$$

where $\langle r^2(t) \rangle$ = mean-square displacement of cellphone users as computed by averaging over a city ensemble of GPS location traces of the motion of M citizens (IDs)

$$\langle r^2(t) \rangle = \frac{1}{M} \sum_{j=1}^{M} r_j^2(t) = \frac{1}{M} \sum_{j=1}^{M} x_j^2(t) + y_j^2(t) \tag{7}$$

and W = proportionality constant having the units of energy (force × length).

The mathematical model appearing in the right-hand side of Eq. (6) was merely constructed by Makris et al. (2023) by using techniques for manipulating signals in radio communication (Gray and Graham 1961; Silver 2011). The function $U(t-0)$ appearing in Eq. (6) is the unit-amplitude Heaviside step-function (Lighthill 1958), $\omega_R = 2\pi/24 = \pi/12$ rad/h is the daily frequency; while parameters A_0, C, and γ are constants of the amplitude-modulation model.

In Eq. (7), $r_j(t)$ is the distance of ID_j from its home H_j at time t. The origin of every ID_j (home H_j) was identified by extracting the most frequent location occupied by ID_j during the time interval from 1:00 AM to 4:00 AM. As an example, Fig. 2 shows East–West (longitude) $x_j(t_k)$ and North–South (latitude) $y_j(t_k)$ displacements of ID_j from its "home" H_j at time t_k. Accordingly, when ID_j moves to the east of its origin (home), H_j, its displacement projection, x_j, is negative; whereas, when it moves to the west of its home, H_j, its displacement projection, x_j, is positive. Similarly, when ID_j moves to the north of its home, H_j, its displacement projection, y_j,

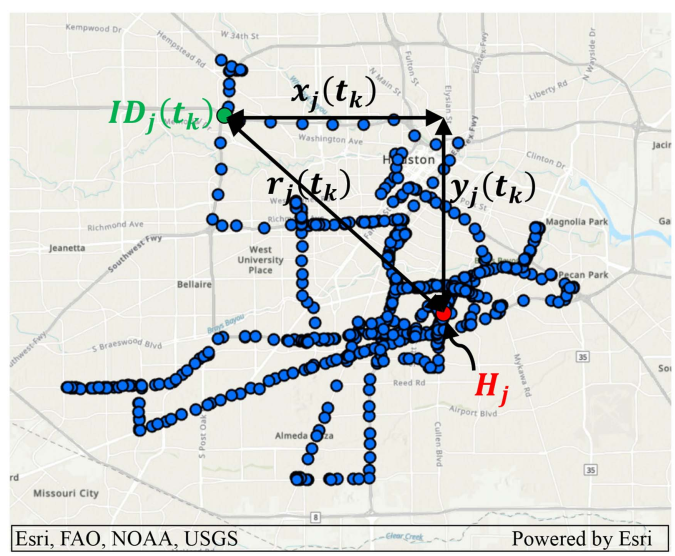

Fig. 2. Displacement $r_j(t_k)$ of ID_j at time t_k from its "home" H_j. In statistical mechanics and microrheology the symbol $\Delta r_j(t_k)$ rather than $r_j(t_k)$ is often used to express the distance of a probe from its "origin". In this work, the symbol Δ is dropped since the displacement r_j is always measured from the fixed origin H_j at all times given that we only work with ensemble averages (not time averages). (Map data from Esri, FAO, NOAA, USGS, Powered by Esri.)

Table 1. GPS location data of M cellphone users (IDs) appearing at the top of each hour of every month

Time	ID_1	ID_2	ID_{j-1}	ID_j	ID_{j+1}	ID_{M-1}	ID_M
t_1	$r_1(t_1)$	$r_2(t_1)$	$\boldsymbol{r_{j-1}(t_1)}$	$r_j(t_1)$	$\boldsymbol{r_{j+1}(t_1)}$	$r_{M-1}(t_1)$	$r_M(t_1)$
t_2	$\boldsymbol{r_1(t_2)}$	$r_2(t_2)$	$r_{j-1}(t_2)$	$r_j(t_2)$	$r_{j+1}(t_2)$	$\boldsymbol{r_{M-1}(t_2)}$	$r_M(t_2)$
t_{k-1}	$r_1(t_{k-1})$	$\boldsymbol{r_2(t_{k-1})}$	$r_{j-1}(t_{k-1})$	$r_j(t_{k-1})$	$\boldsymbol{r_{j+1}(t_{k-1})}$	$r_{M-1}(t_{k-1})$	$r_M(t_{k-1})$
t_k	$\boldsymbol{r_1(t_k)}$	$r_2(t_k)$	$r_{j-1}(t_k)$	$r_j(t_k)$	$r_{j+1}(t_k)$	$r_{M-1}(t_k)$	$\boldsymbol{r_M(t_k)}$
t_{k+1}	$r_1(t_{k+1})$	$r_2(t_{k+1})$	$r_{j-1}(t_{k+1})$	$\boldsymbol{r_j(t_{k+1})}$	$r_{j+1}(t_{k+1})$	$\boldsymbol{r_{M-1}(t_{k+1})}$	$r_M(t_{k+1})$
t_{719}	$r_1(t_{719})$	$\boldsymbol{r_2(t_{719})}$	$r_{j-1}(t_{719})$	$r_j(t_{719})$	$\boldsymbol{r_{j+1}(t_{719})}$	$r_{M-1}(t_{719})$	$r_M(t_{719})$
t_{720}	$r_1(t_{720})$	$r_2(t_{720})$	$\boldsymbol{r_{j-1}(t_{720})}$	$r_j(t_{720})$	$r_{j+1}(t_{720})$	$r_{M-1}(t_{720})$	$r_M(t_{720})$
				and for a month with 31 days			
t_{721}	$r_1(t_{721})$	$\boldsymbol{r_2(t_{721})}$	$r_{j-1}(t_{721})$	$\boldsymbol{r_j(t_{721})}$	$r_{j+1}(t_{721})$	$r_{M-1}(t_{721})$	$r_M(t_{721})$
t_{743}	$r_1(t_{743})$	$r_2(t_{743})$	$r_{j-1}(t_{743})$	$\boldsymbol{r_j(t_{743})}$	$r_{j+1}(t_{743})$	$r_{M-1}(t_{743})$	$r_M(t_{743})$
t_{744}	$\boldsymbol{r_1(t_{744})}$	$r_2(t_{744})$	$r_{j-1}(t_{744})$	$r_j(t_{744})$	$r_{j+1}(t_{744})$	$r_{M-1}(t_{744})$	$\boldsymbol{r_M(t_{744})}$

Note: Entries in boldface are indicative missing entries when an ID needs to appear only at least $P < 720$ (or $P < 744$) times at the top of the hour in a given month.

is positive; whereas, when it moves to the south of its home, H_j, its displacement projection, y_j, is negative. For every city, the GPS location data of a large number of IDs (hundreds of thousands to millions) are distilled to retrieve the IDs that appear close to the top of every hour for every day in a given month–that is $24\ (\mathrm{h/day}) \times 30\ (\mathrm{days/month}) = 720$ appearance/month or $24\ (\mathrm{h/day}) \times 31\ (\mathrm{days/month}) = 744$ appearance per month. For every city and every month, the displacements $r_j(t_k) = \sqrt{x_j^2(t_k) + y_j^2(t_k)}$ of each ID_j at time t_k are organized as shown in Table 1.

Fig. 3 plots the time history of the mean-square displacement $\mathrm{MSD} = \langle r^2(t) \rangle$ as defined by Eq. (7) of $M = 1409$ IDs for August, $M = 1712$ IDs for September and $M = 1999$ IDs for October 2020 in the greater Miami area shown in Fig. 4 that appeared close to the top of the hour during the entire duration of each month. Fig. 3 reveals that the MSD for the city of Miami exhibits a remarkable periodicity with people moving more during the weekdays and less on Sundays that are marked with green dots. At the same time, fewer people are staying at home during the weekends than during

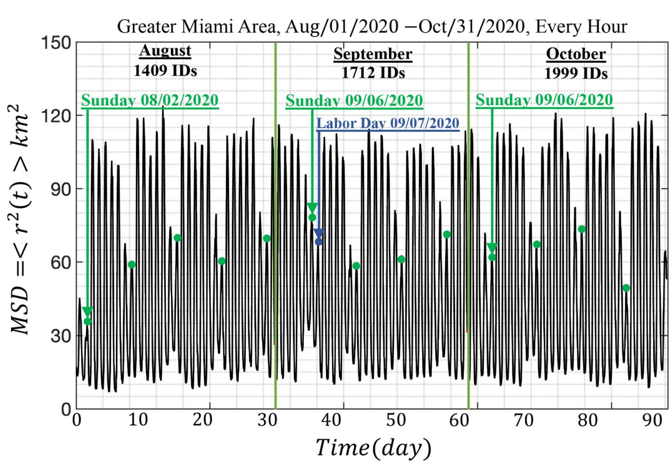

Fig. 3. Time history of the mean-square displacement $= \langle r^2(t) \rangle = \frac{1}{M} \sum_{j=1}^{M} r_j^2(t)$ (ensemble average) of $M = 1{,}409$ for August, $M = 1{,}712$ IDs for September, and $M = 1{,}999$ IDs for October 2020, in the Miami greater area of Florida under normal steady-state operational conditions (no event). Dots atop the suppressed spikes indicate Sundays.

the weekdays. Accordingly, in the steady-state regime of the city of Miami together with the daily oscillations with frequency $\omega_R = 2\pi/24 = \pi/12$ rad/h (carrier wave), there is a weekly modulation (message signal). This amplitude-modulation steady-state response of the MSD of cities as depicted in Fig. 3 is captured with the amplitude-modulation model appearing on the right of Eq. (6) (Makris et al. 2023). Fig. 5 compares the recorded $\mathrm{MSD} = \langle r^2(t) \rangle$ from the city of Miami shown in Fig. 3 with the predictions of the calibrated amplitude-modulation model given by Eq. (6) with $A_0 = 60\ \mathrm{km}^2$, $C = 0.7$, and $\gamma = 0.25$.

The requirement for an ID_j to appear at the top of every hour every day for all 30 or 31 days in a month is a very demanding requirement and we lose many IDs that have a nearly perfect appearance over the duration of the month. Accordingly, for cities and years where the number M of IDs that occupy all the cells of Table 1 becomes low (say $M < 360$), the requirement for 720 or 744 appearances in a month is relaxed to a lower yet significant threshold number (say at least $P = 700$ or sometimes down to at least $P = 540$ appearances in a month)—that is, each column of Table 1 needs to show at least $P = 700$ or $P = 540$ (depending on the threshold value, P) nonempty cells. With this relaxation, IDs that their displacements $r_j(t_k)$ are missing in Table 1 are included as long as the appearances of any ID_j is above the threshold number P. As an example, Fig. 6 plots the time history of the mean-square displacement $\mathrm{MSD} = \langle r^2(t) \rangle$ of cellphone users in the greater Jacksonville area in Florida shown in Fig. 7 during $Q3$ and $Q4$ of 2021 that appeared close to the top of the hour during the entire duration of each month at least $P = 600$ times. As shown in Fig. 6, in this way we can distill a large number of valuable IDs (at least 600 appearances per month) ranging from 26,072 IDs in the month of November 2021 to 30,709 IDs in the month of August 2021.

With this relaxation, the number of IDs in an ensemble, $M(t_k)$, (IDs appearing along each row of Table 1) becomes time-dependent, and Eq. (7) is expressed as

$$\langle r^2(t_k) \rangle = \frac{1}{M(t_k)} \sum_{j=1}^{M(t_k)} r_j^2(t) = \frac{1}{M(t_k)} \sum_{j=1}^{M(t_k)} x_j^2(t) + y_j^2(t) \qquad (8)$$

Fig. 8 compares the recorded $\mathrm{MSD} = \langle r^2(t) \rangle$ from the greater Jacksonville, Florida, area shown in Fig. 7 under normal steady-state operational conditions (No event) with the predictions of the calibrated amplitude-modulation model given by Eq. (6) with $A_0 = 90\ \mathrm{km}^2$, $C = 0.6$, and $\gamma = 0.35$.

J. Eng. Mech., 2023, 149(10): 04023076

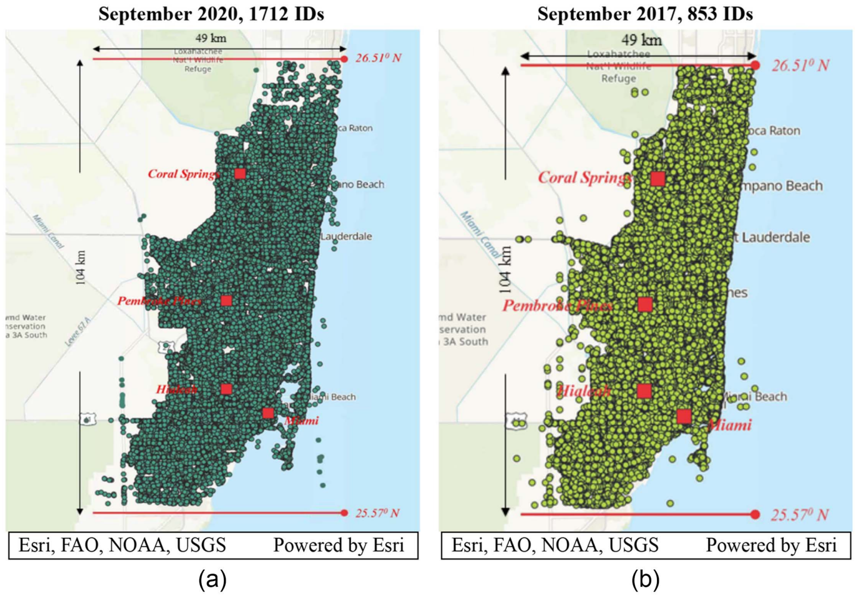

Fig. 4. GPS locations of anonymous cellphone users (IDs) in the greater Miami area recorded during (a) September 2020 (normal conditions with no event. 1712 IDs recorded at the top of each hour); and (b) September 2017 when the greater Miami area was hit by category 5 hurricane Irma. 853 IDs recorded at the top of each hour with at least 540 appearances during the month of September 2017 ($P = 540$). (Map data from Esri, FAO, NOAA, USGS, Powered by Esri.)

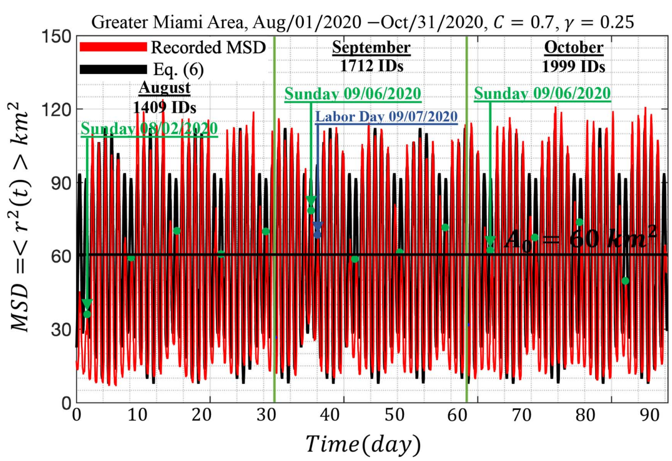

Fig. 5. Comparison of the predictions of the calibrated amplitude-modulation analytical expression of $\langle r^2(t) \rangle$ given by Eq. (6) with the recorded mean-square displacement of the citizens of Miami under normal, steady-state operational conditions (no event) during the months of August, September, and October 2020 shown in Fig. 3.

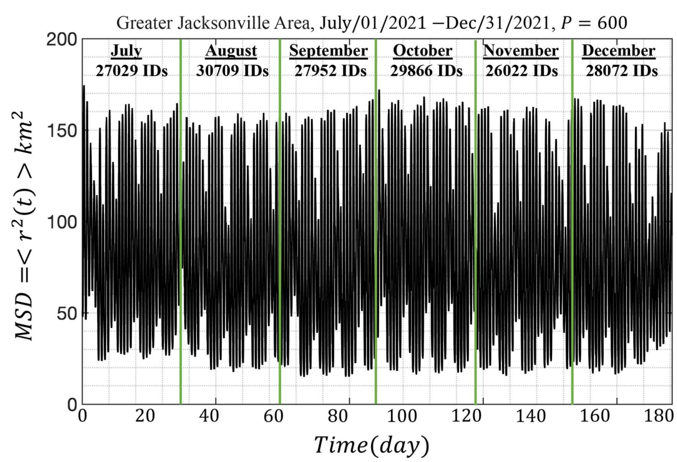

Fig. 6. Time history of the mean-square displacement $= \langle r^2(t) \rangle$ (ensemble average) of IDs that have at least $P = 600$ appearances every month close to the top of the hour in the Jacksonville, Florida, greeter area under normal, steady-state operational conditions (No event) during the $Q3$ and $Q4$ of 2021.

Response of Large Cities to Natural Hazards

Urban resilience in this work is investigated and quantified by studying: (1) the response of the Dallas and Houston metroplexes that were subjected to the February 2021 North American winter storm, and (2) the response of three large US cities (Houston, Miami, and Jacksonville) when subjected to category 4 and 5 hurricanes.

The February 2021 North American Winter Storm

The North American winter storm happened during the 3rd week of February 2021 and ended sometime toward the end of that week before Sunday, February 21, 2021 (National Weather Service 2021; NOAA 2021). Over 4 million people lost power due to the storm which resulted in a state-wide crisis in Texas causing major damage to the Texas power grid.

Fig. 9 plots the time history of the mean-square displacement $\mathrm{MSD} = \langle r^2(t) \rangle$ as defined by Eq. (8) of $M = 30373$ IDs for January with $P = 720$, $M = 34921$ IDs for February with $P = 650$ and $M = 25257$ IDs for March with $P = 720$ of year 2021 in the Dallas metroplex that appeared close to the top of each hour during the entire duration of each month.

Fig. 9 reveals that while the MSD for the Dallas metroplex exhibits the same daily and weekly periodicity that emerges from the city of Miami shown in Figs. 3 and 5 and the city of Jacksonville

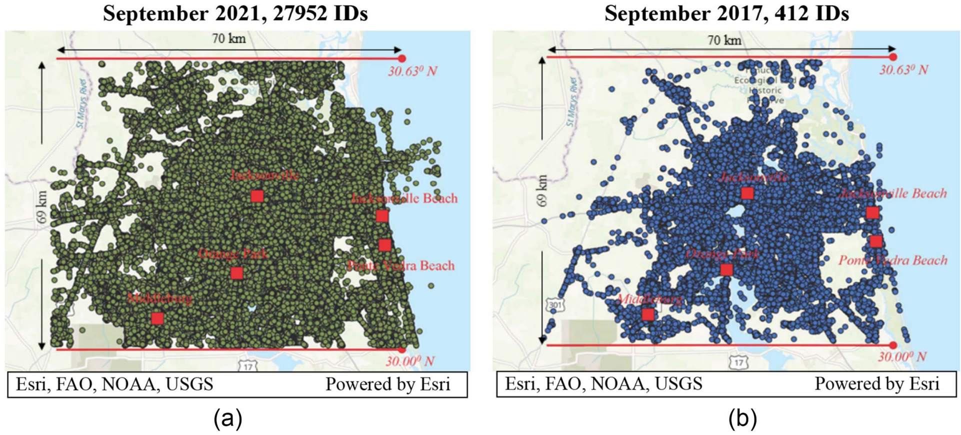

Fig. 7. GPS locations of anonymous cellphone users (IDs) in the greater Jacksonville area recorded during (a) September 2021 (normal conditions with No event: 27952 IDs with $P = 600$); and (b) September 2017 when the greater Jacksonville area was hit by category 5 hurricane Irma. 412 IDs recorded at the top of each hour with at least 540 appearances during the month of September 2017 ($P = 540$). (Map data from Esri, FAO, NOAA, USGS, Powered by Esri.)

shown in Figs. 6 and 8, it also exhibits a noticeable suppression during the duration of the North American winter storm. Fig. 9 shows that immediately after the expiration of the cold winter storm [sometime by Saturday, February 20, 2021 (NOAA 2021; National Weather Service 2021)], the city of Dallas resumes normal activity with the MSD of its citizens to revert to its normal oscillation pattern as recorded before the storm, suggesting that the Dallas metroplex exhibits a great degree of engineering resilience as defined by Holling (1996). The prediction for the response of the Dallas metroplex following the North American winter storm with the amplitude-modulation model given by Eq. (6) has been presented in Makris et al. (2023).

The same inherent and immediate resilience to the 2021 North American winter storm manifested by the city of Dallas is also manifested by city of Houston, Texas, and also resumes normal activity upon the expiration of the winter storm with the MSD of its citizens to revert to its normal oscillation pattern as shown in Fig. 10. The number of distilled IDs that appear at the top of the hour for the duration of each month of $Q1$ of 2021 is also shown in Fig. 10.

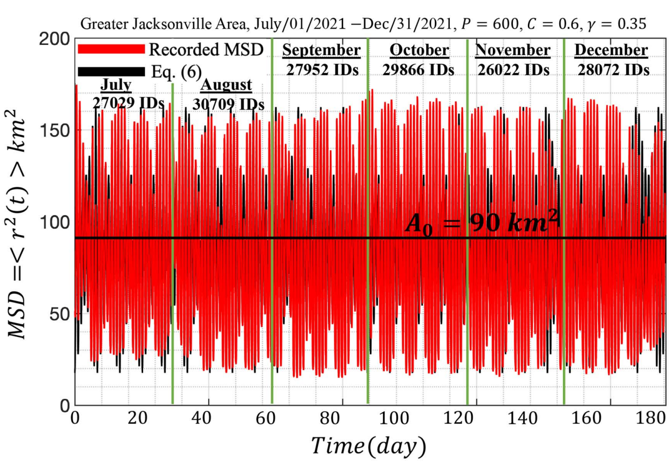

Fig. 8. Comparison of the predictions of the calibrated amplitude-modulation analytical expression of $\langle r^2(t)\rangle$ given by Eq. (6) with the recorded mean-square displacement, $r^2(t)$, of the citizens of Jacksonville, Florida under normal, steady-state operational conditions (No event) during the $Q3$ and $Q4$ of 2021 shown in Fig. 6.

Fig. 11 compares the recorded MSD $= \langle r^2(t)\rangle$ of the citizens in the greater Houston area during $Q1$ of 2021 shown in Fig. 10 with the predictions of the calibrated amplitude-modulation model given by Eq. (6) under normal steady-state operating conditions with $A_0 = 80\ \mathrm{km}^2$, $C = 0.6$, and $\gamma = 0.25$.

In the next section, we show that the amplitude-modulation model, as conjectured by Eq. (6), predicts that the postevent behavior of the MSD of a large city is indeed identical to its preevent behavior as revealed by the recorded MSDs shown in Figs. 9 and 10. Fig. 11 plots the time history of the mean-square displacement of cellphone users in the greater Houston area shown in Fig. 12 that were recorded during the period January 1 to March 31, 2021.

Prediction of the Measured Postevent Regime of Cities

In view of the satisfactory performance of the analytical expression offered by Eq. (6) to capture the steady-state regime of cities under normal, operating conditions as shown in Fig. 5 for the regime of Miami and Fig. 8 for the regime of Jacksonville, in this section; we validate the conjecture described by Eq. (6)—that the mechanical model with creep compliance

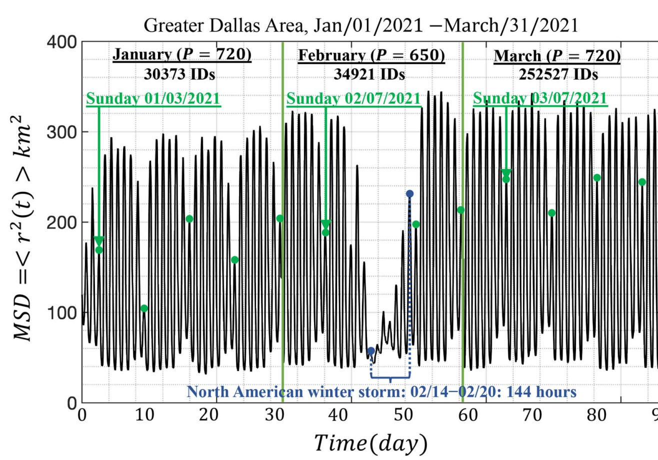

Fig. 9. Time history of the mean-square displacement $= \langle r^2(t)\rangle$ (ensemble average) of cellphone IDs in the Dallas metroplex during $Q1$ of 2021. Dots atop the suppressed spikes indicate Sundays.

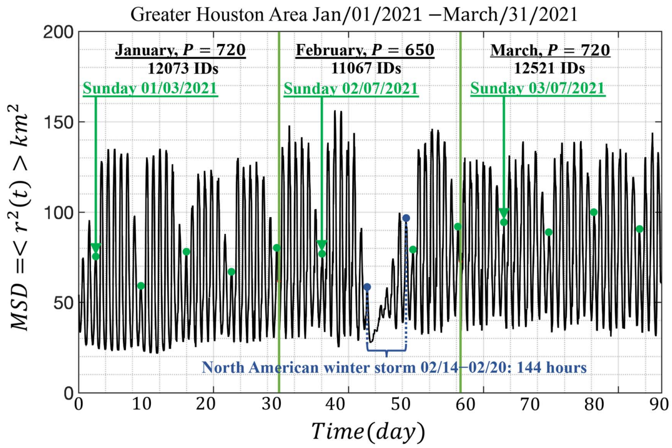

Fig. 10. Time history of the mean-square displacement $= \langle r^2(t)\rangle$ (ensemble average) of cellphone IDs in the greater Houston area during $Q1$ of 2021. Dots atop the suppressed spikes indicate Sundays.

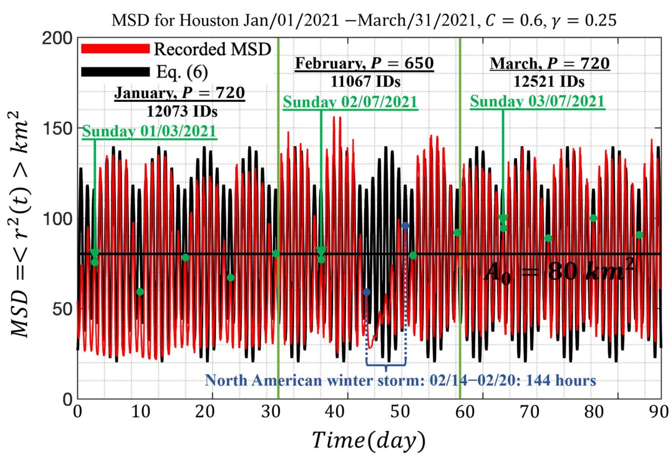

Fig. 11. Comparison of the predictions of calibrated amplitude-modulation analytical expression of $\langle r^2(t)\rangle$ given by Eq. (6) under normal steady-state operational conditions (no event) in the greater Houston area with the recorded mean-square displacement $\langle r^2(t)\rangle$ of the citizens of Houston, Texas during $Q1$ of 2021 shown in Fig. 10.

$$J(t) = \frac{\langle r^2(t)\rangle}{A_0 k} = \frac{1}{k}\left\{U(t-0) - C\left[\cos(\omega_R t) + \frac{\gamma}{2}\left(\sin\left(\frac{8}{7}\omega_R t\right) - \sin\left(\frac{6}{7}\omega_R t\right)\right)\right]\right\} \tag{9}$$

is indeed a mechanical analog for cities that predicts with remarkable fidelity the postevent regime of cities (Makris et al. 2023). In Eq. (9), $k = W/A_0$ is a constant with units of stiffness ($[F]/[L]$).

In our analysis, natural hazards such as earthquakes, hurricanes, and winter storms that start and end abruptly and are system wide are represented mathematically with an elementary rectangular pulse of amplitude F_0 and duration T_e which is expressed as

$$F(t) = F_0[U(t-0) - U(t-T_e)] \tag{10}$$

where $U(t-\xi)$ = unit-amplitude Heaviside step-function that initiates at time $t = \xi$ (Lighthill 1958). Other societal stressors such as pandemics and economic crises are stressing cities during larger time scales along which the city may develop mechanisms to readjust (Meerow et al. 2016). Accordingly, for such prolonged crises that ramp-up gradually and may have long tails, different loading patterns than the rectangular pulse described in Eq. (10) may be more suitable.

The creep compliance, $J(t)$ (displacement history due to a unit-step force), is a time-response function of a linear system. Given the linearity of the mechanical model for a city as expressed by Eqs. (6) or (9); the response, $u(t)$, of the mechanical model due to a force excitation $F(t)$ is offered through the convolution integral

$$u(t) = \int_{0^-}^{t} h(t-\xi)F(\xi)d\xi \tag{11}$$

where $F(\xi)$ = time history of the acute shock—in this analysis the rectangular pulse given by Eq. (10); and $h(t)$ = impulse response function (Clough and Penzien 1970; Oppenheim and Schafer 1975; Harris and Crede 1976; Reid 1983; Makris 2021a) that is defined as the resulting displacement history, $u(t)$, due to an impulsive force input $F(t) = \delta(t-\xi)$ with $\xi < t$. Given that $\delta(t-\xi) = dU(t-\xi)/dt$, the impulse response function of a linear system $h(t) = dJ(t)/dt$ where $J(t)$ is its creep compliance (displacement history due to a unit-step force). Accordingly, the impulse response function of the mechanical model of a city described in Eq. (6) is

$$h(t) = \frac{dJ(t)}{dt} = \frac{1}{k}\left\{\delta(t-0) + C\omega_R\left[\sin(\omega_R t) - \frac{\gamma}{2}\left(\frac{8}{7}\cos\left(\frac{8}{7}\omega_R t\right) - \frac{6}{7}\cos\left(\frac{6}{7}\omega_R t\right)\right)\right]\right\} \tag{12}$$

Substitution of the expression of the impulse response function given by Eq. (12) into Eq. (11) after using the forcing function $F(\xi)$ as expressed by Eq. (10), the normalized displacement response from the amplitude-modulation model when subjected to a rectangular pulse of duration T_e is (Makris et al. 2023)

$$\frac{k}{F_0}u(t) = U(t-0) - U(t-T_e) + C\left[-\cos(\omega_R t) + \cos(\omega_R(t-T_e)) - \frac{\gamma}{2}\left(\sin\left(\frac{8}{7}\omega_R t\right) - \sin\left(\frac{8}{7}\omega_R(t-T_e)\right) - \sin\left(\frac{6}{7}\omega_R t\right) + \sin\left(\frac{6}{7}\omega_R(t-T_e)\right)\right)\right] \tag{13}$$

With reference to Figs. 10 or 11, prior to the arrival of the North American winter storm, the city of Houston, Texas, was operating under normal conditions, and its mean-square displacement $\langle r^2(t)\rangle$ of its citizens is described satisfactorily with the amplitude-modulation model given by Eq. (6) and plotted at the top of Fig. 13(a) (see also Fig. 11). While Houston was operating under normal conditions, on Sunday Feb 14, $t_0 = 0$, it was suddenly subjected to the North American winter storm that is described with the rectangular pulse with a duration $T_e = (6\text{ days}) \times (24\text{ h/day}) = 144$ hour*s* as shown in Fig. 13(b) that is the duration reported by the media (National Weather Service 2021). The overall response upon the city of Houston is subjected to the acute cold storm (postevent response) is the superposition of its steady-state response under normal operating conditions given by Eq. (6) and shown in Fig. 13(a) and its response due to the rectangular pulse

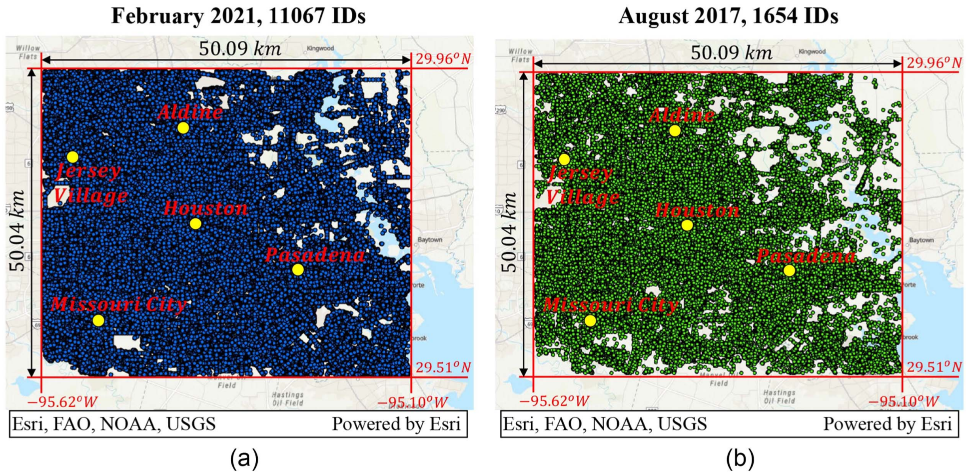

Fig. 12. GPS locations of anonymous cellphone users (IDs) in the greater Houston area recorded during: (a) February 2021 when Houston was hit by a North America Winter Storm. 11067 IDs with $P = 650$; and (b) August 2017 when Houston was hit by hurricane Hervey. 1654 IDs with $P = 540$. (Map data from Esri, FAO, NOAA, USGS, Powered by Esri.)

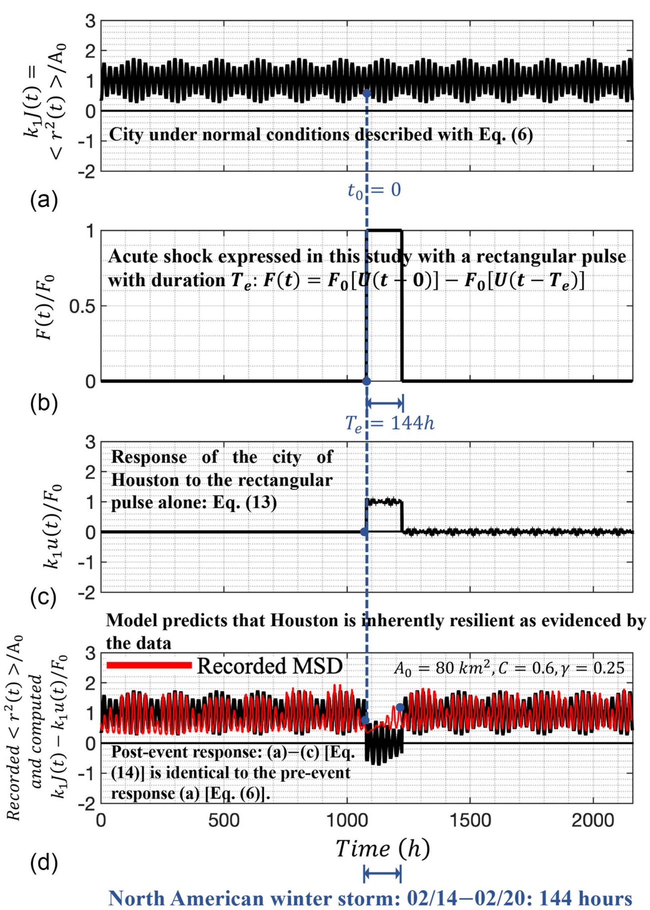

Fig. 13. (a) Normalized behavior of the city of Houston under normal conditions as given by Eq. (6); (b) acute shock on a city expressed with a rectangular pulse with duration $T_e = 144$ h that is an integer multiple of a day $= 24$ h; (c) normalized response of the city of Houston to the rectangular pulse alone with duration $T_e = 144$ h; and (d) pre- and postevent response of Houston [(a–c), solid dark lines] which is identical to the preevent response of Houston (a). The thin red lines are the normalized recorded MSD of the Houston metroplex prior to, during, and after the North American winter storm during the 3rd week of February 2021 as distilled from the recorded GPS location data.

given by Eq. (14) and shown in Fig. 13(c). Accordingly, the "post-event" response of a city described with the amplitude-modulation model given by Eq. (6) is

$$kJ(t) - \frac{k}{F_0}u(t) = U(t-T_e) - C\Bigg[\cos(\omega_R(t-T_e)) + \frac{\gamma}{2}\left(\sin\left(\frac{8}{7}\omega_R(t-T_e)\right) - \sin\left(\frac{6}{7}\omega_R(t-T_e)\right)\right)\Bigg] \tag{14}$$

The right-hand side of Eq. (14) that results after subtracting Eqs. (13) from (6) is precisely of the same form as Eq. (6) and reveals that upon the expiration of the acute shock (rectangular pulse), the amplitude-modulation model predicts that the city reverts immediately to its normal preevent activities (identical $\langle r^2(t)\rangle$ as before the acute shock) as evidenced by the recorded MSD of the Dallas metroplex shown in Fig. 9 and the greater Houston area shown in Figs. 10 and 11. When the duration of the rectangular pulse is an integer multiple of a day as shown in Fig. 13(b), the sine functions appearing in Eq. (13) do not cancel because of the multiplication factors 8/7 and 6/7, resulting in the small undulations that override the rectangular pulse response shown in Fig. 13(c). The small undulations cancel only when $T_e = 7$ days $= 1$ week $= 168$ h as shown in Fig. 14(c).

Estimation of the Recovery Time of a City by Synchronizing the Recorded and Predicted MSDs

Fig. 13(d) shows that when we used as the duration of the rectangular pulse $T_e = 144$ h, which is the duration reported by the media (National Weather Service 2021) as the predicted response of Houston's MSD following the storm is identical to the preevent MSD, yet it appears that the predicted postevent MSD is approximately one day out of phase of the recorded MSD. This one extra day is the time that the greater Houston area needed to fully recover from the February 2021 North American winter storm.

Fig. 14 shows the predicted preevent and postevent response of the city of Houston when the duration of excitation of the rectangular pulse is $T_e = (7\text{days}) \times (24\text{ h/day}) = 168$ h and shows that for this pulse-duration $T_e = 168$ h, the predicted postevent MSD synchronizes with the recorded postevent MSD, indicating that the

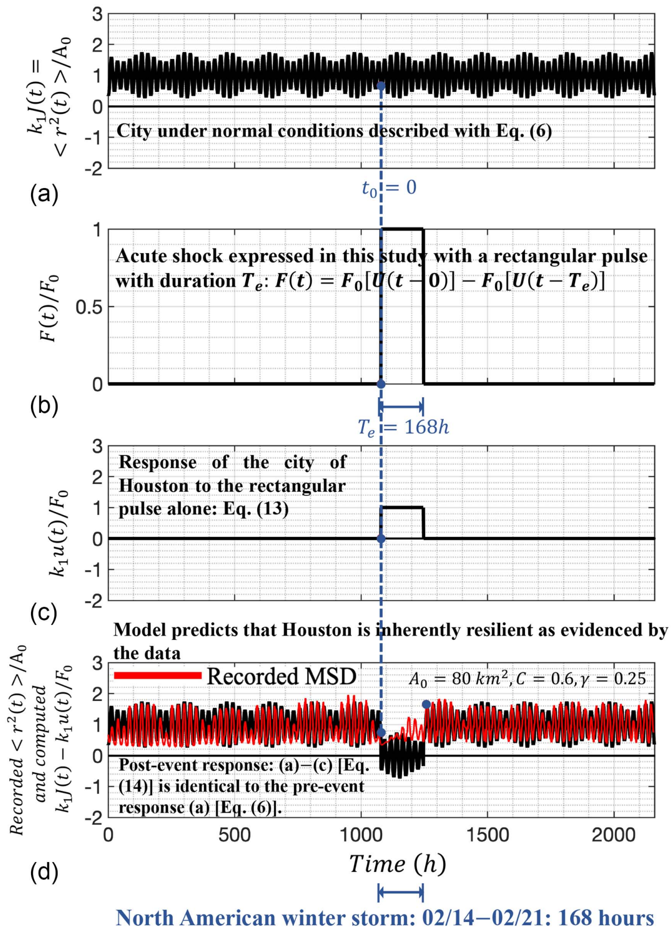

Fig. 14. (a) Normalized behavior of the city of Houston under normal conditions as given by Eq. (6); (b) acute shock on a city expressed with a rectangular pulse with a duration $T_e = 168$ h that is an integer multiple of a day $= 24$ h; (c) normalized response of the city of Houston to the rectangular pulse alone with duration $T_e = 168$ h; and (d) preevent and postevent response of Houston [(a–c), solid dark lines] which is identical to the preevent response of Houston (a). The thin red lines are the normalized recorded MSD of the Houston metroplex prior to, during, and after the North American winter storm during the 3rd week of February 2021 as distilled from the recorded GPS location data.

recovery time of the greater Houston area to the February 2021 North American winter storm was of the order of a single day. Accordingly, the postevent synchronization of the recorded and predicted MSD allows us to estimate the recovery time of an urban center with an accuracy of the order of $1/2$ day $= 12$ h.

The August 2017 Hurricane Harvey

The inherent resilience of a city is evidenced by the recovery of the mean-square displacement of its citizens immediately after the expiration of the natural hazard, as shown in Fig. 9 for the Dallas metroplex and Figs. 10 and 11 for the greater Houston area when hit by the 2021 North American winter storm, and is examined for more intense natural hazards known to have created unprecedented damage.

Hurricane Harvey was a category 4 storm that hit Texas on August 25, 2017, and made landfall three times in six days (Amadeo 2018). Together with the 2017 Hurricane Irma, it is considered the 1,000-year return period of precipitation extreme

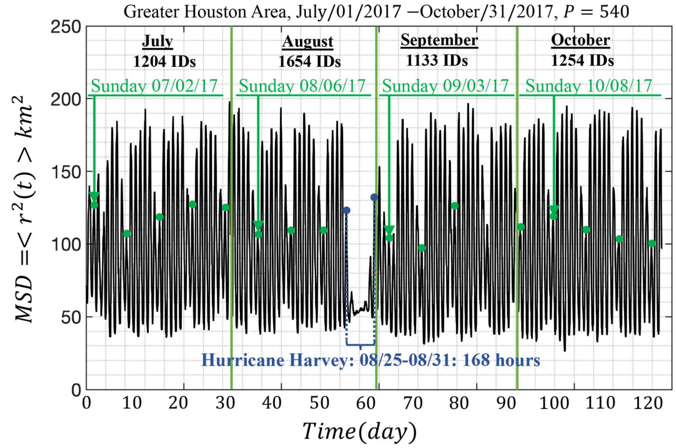

Fig. 15. Time history of the mean-square displacement $= \langle r^2(t)\rangle$ (ensemble average) of cellphone IDs in the greater Houston area which appeared at least $P = 540$ times per month during the period July 1, to October 31, 2017. Dots atop the suppressed spikes indicate Sundays.

(Vu and Mishra 2019). By the end of August 2017, one-third of Houston was under, water forcing close to 30,000 people out of their homes into shelters. Loses from damage exceeding \$100 billion—that is more than any other natural disaster in US history other than hurricane Katrina back in August 2005. Nevertheless, cellular phone service in Houston remained functional despite isolated outages with only 3.5% of cellular towers in Harris County to go down; while in Nueces County, 19% of its cellular towers were not working (Ehlinger 2017).

Fig. 15 plots the time history of the mean-square displacement, $\langle r^2(t)\rangle$, of cellphone users in the greater Houston area shown in Fig. 12 that were recorded during the period July 1 to October 31, 2017, and appeared close to the top of the hour at least $P = 540$ times during the entire duration of each month. In spite of the unprecedented damage inflicted by Hurricane Harvey in the greater Houston area, Fig. 15 reveals that immediately after the passage of Hurricane Harvey (August 31, 2017) the city of Houston resumes its normal, preevent activity with the MSD of its citizens to revert to its normal oscillation pattern as recorded before the hurricane, suggesting that the greater Houston area exhibits a great degree of engineering resilience as defined by Holling (1996).

Fig. 16 compares the recorded MSD $= \langle r^2(t)\rangle$ of the citizens in the greater Houston area during the period July 1 to October 31, 2017, shown in Fig. 15 with the predictions of the calibrated, amplitude-modulation model given by Eq. (6) under normal, steady-state operating conditions (No event) with $A_0 = 110$ km^2, $C = 0.6$, and $\gamma = 0.25$. An interesting observation is that while the values of parameters $C = 0.6$ and $\gamma = 0.25$ for the greater Houston area are the same for years 2021 (Fig. 11) and 2017 (Fig. 16), the mean value of the MSD $= 80$ km^2 for year 2021 is smaller than the mean value of the MSD $= 110$ km^2 for year 2017.

This suggests that less average area is covered on average by the citizens of Houston in year 2021 than in year 2017, which may be due to changes in the commuting patterns following the postpandemic era.

Prediction of the Houston MSD Following Hurricane Harvey

With reference to Figs. 15 and 16, prior to Hurricane Harvey's landfall, the greater Houston area was operating under normal

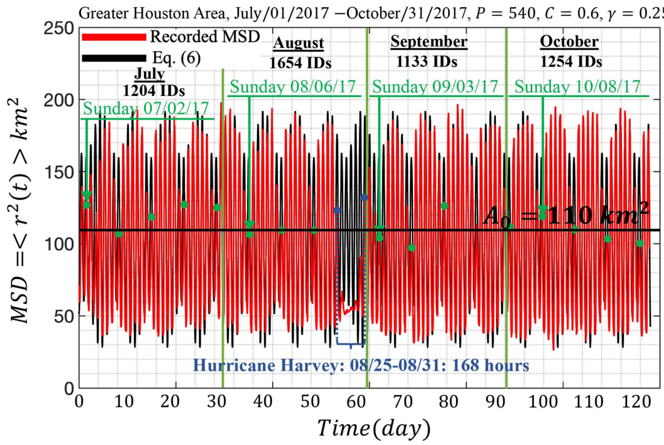

Fig. 16. Comparison of the predictions of the amplitude-modulation model ($A_0 = 110$ km^2, $C = 0.6$ and $\gamma = 0.25$) given by Eq. (6) under normal steady-state operational conditions (no event) in the greater Houston area with the recorded mean-square displacement $\langle r^2(t) \rangle$ of the distilled number of IDs shown in the figure for each month during the period July 1, to October 31, 2017.

conditions, and its mean-square displacement, $\langle r^2(t) \rangle$, of its citizens is described satisfactorily with the amplitude-modulation model given by Eqs. (6) or (9) and plotted in Fig. 17(a) (see also Fig. 16). While Houston was operating under normal conditions, on August 25, 2017, $t_0 = 0$, Hurricane Harvey struck Houston for some 7 days and this intense loading to its population and infrastructure is described with a rectangular pulse with duration $T_e =$ 168 hours as shown in Fig. 17(b).

The response of the greater Houston area to the rectangular pulse shown in Fig. 17(b) is offered by Eq. (13) and is plotted in Fig. 17(c). The overall response of the greater Houston area following the response to Hurricane Harvey (postevent response) is the superposition of its steady-state response under normal conditions and its response due to the rectangular pulse as described by Eq. (14) and plotted in Fig. 17(d) following the expiration of the rectangular pulse. Eq. (14) predicts the immediate recovery of the MSD $= \langle r^2(t) \rangle$ of the citizens of Houston as evidenced by the recorded MSD shown in Fig. 15 because the right-hand side of Eq. (14) is precisely of the same form as Eq. (6).

By selecting a duration of the rectangular pulse, $T_e = 7\text{days} =$ 168 h the predicted postevent response is perfectly synchronized with the recorded postevent response as shown in Fig. 17(d). Given that August 31, 2017, was a Thursday, the recorded MSD shown in Figs. 15, 16, and 17(d) shows that the greater Houston area had reverted to its normal prehurricane behavior by Saturday, September 02, 2017, demonstrating a remarkable engineering resilience (Holling 1996).

The September 2017 Hurricane Irma

Following Hurricane Harvey, in less than two weeks, category 5 Atlantic Hurricane Irma hit Miami on September 9, 2017, creating widespread power outages. The storm surge caused coastal flooding from Homestead to downtown Miami and portions of Miami Beach (Tropical Winds Newsletter 2017). Hurricane Irma is the fifth costliest hurricane to hit the mainland United States and caused an estimated \$50 billion in damage according to the National Hurricane Center (Huber 2018).

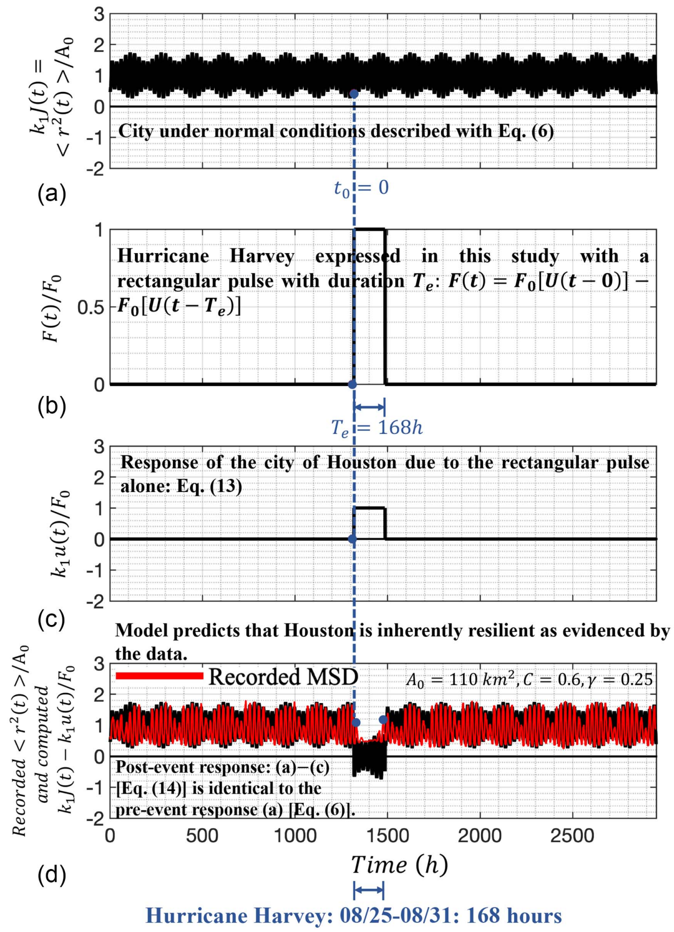

Fig. 17. (a) Normalized behavior of the city of Houston under normal conditions as given by Eq. (6); (b) acute shock on a city expressed with a rectangular pulse with a duration $T_e = 168$ h that is an integer multiple of a day = 24 h; (c) normalized response of the city of Houston to the rectangular pulse alone with duration $T_e = 168$ h; and (d) pre- and postevent response of Houston [(a–c), solid dark lines] which is identical to the preevent response of the city (a). The thin red lines are the normalized recorded MSD of the Houston greater area prior to, during, and after Hurricane Harvey which happened in late August 2017 as distilled from the recorded GPS location data.

Fig. 18 plots the time history of the mean-square displacement $= \langle r^2(t) \rangle$ of cellphone users in the greater Miami area shown in Fig. 4 that were recorded during the period July 1, to December 31, 2017, and appeared close to the top of the hour at least $P =$ 540 times during the entire duration of each month. Fig. 19 compares the recorded MSD $= \langle r^2(t) \rangle$ of the citizens in the greater Miami area during the period July 1 to December 31, 2017, shown in Fig. 18 with the predictions of the calibrated, amplitude-modulation model given by Eqs. (6) or (9) under normal steady-state operating conditions (no event) with $A_0 = 95$ km^2, $C = 0.6$, and $\gamma = 0.25$.

In agreement with the observations reported upon examining the recorded MSDs of Houston, the mean value of the MSD = 60 km^2 of the greater Miami area during 2020 shown in Fig. 5 is smaller than the mean value of the MSD = 95 km^2 of the greater Miami area during 2017, as shown in Fig. 19. The smaller average area covered by the citizens of Miami in year 2020 (60 km^2) reflects the changes in the commuting patterns of the citizens during the pandemic era.

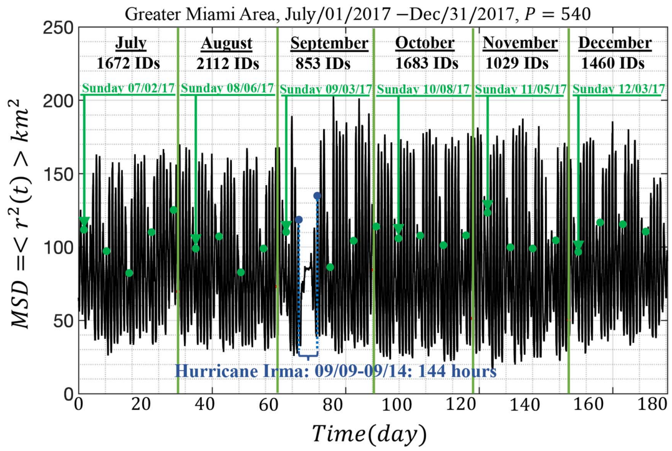

Fig. 18. Time history of the mean-square displacement $= \langle r^2(t) \rangle$ (ensemble average) of cellphone IDs in the greater Miami area which appeared at least $P = 540$ times per month during the period July 1, to December 31, 2017. Dots atop the suppressed spikes indicate Sundays.

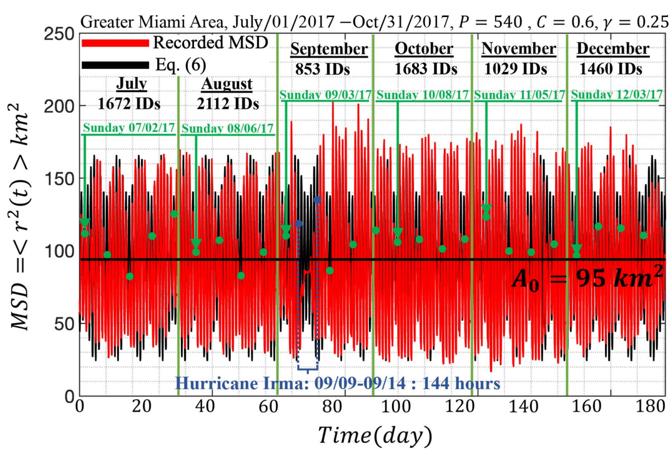

Fig. 19. Comparison of the predictions of the amplitude-modulation model ($A_0 = 95\ \mathrm{km}^2$, $C = 0.6$ and $\gamma = 0.25$) given by Eq. (6) under normal steady-state operational conditions (no event) in the greater Miami area with the recorded mean-square displacement $\langle r^2(t) \rangle$ of the distilled number of IDs shown in the figure for each month during the period July 1, to December 31, 2017.

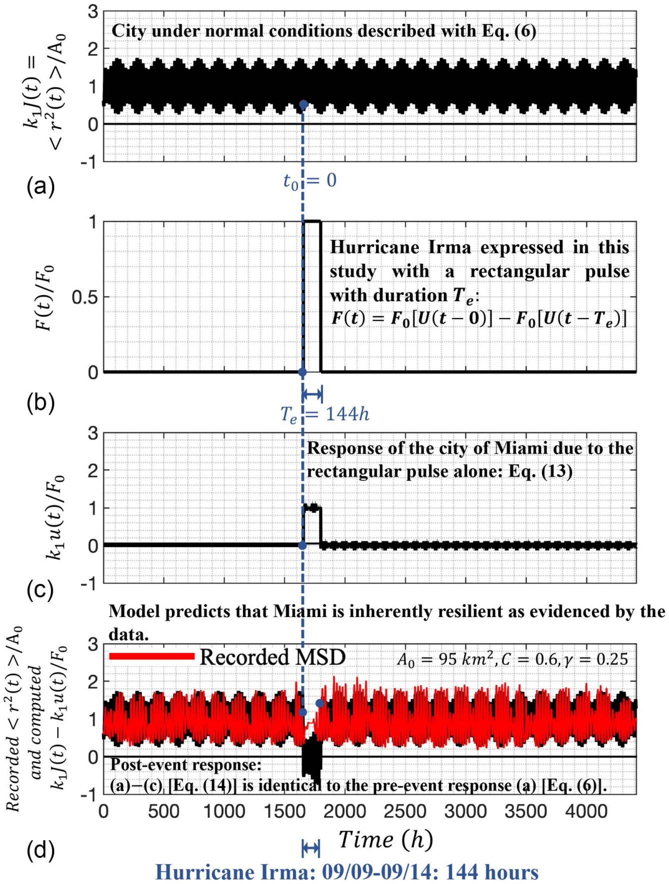

Fig. 20. (a) Normalized behavior of the city of Miami under normal conditions as given by Eq. (6); (b) acute shock on a city expressed with a rectangular pulse with a duration $T_e = 144$ h that is an integer multiple of a day $= 24$ h; (c) normalized response of the city of Miami to the rectangular pulse alone with duration $T_e = 144$ h; and (d) preevent and postevent response of Miami [(a–c), solid dark lines] which is identical to the preevent response of the city (a). The thin red lines are the normalized MSD of the Miami metroplex prior to, during, and after Hurricane Irma which happened in September 2017 as computed from the recorded GPS location data.

Fig. 20 plots for the greater Miami area the corresponding plots appearing in Fig. 17 that were analyzed in detail for the city of Houston when hit by Hurricane Harvey and reveals that our analytical model expressed with Eqs. (6) or (9) that yields Eq. (14) captures the recorded posthurricane response of the city of Miami with remarkable accuracy as shown in Fig. 20(d). The posthurricane recorded and predicted MSDs are perfectly synchronized, revealing that the greater Miami area reverted immediately to its postevent regime confirming our thesis that large urban centers exhibit an inherent engineering resilience.

Upon hurricane Irma hit the greater Miami area it climbed to the north by staying close to the west coast of the Florida peninsula. Nevertheless, from September 9 to 14, the city of Jacksonville on the east coast (Atlantic coast) experienced a tropical storm that created power outages for more than 260,000 citizens in the greater Jacksonville area. A combination of storm surges, high tides, and heavy rainfall caused record water levels in St. Johns Rivers that resulted in major flooding (Stepzinski 2017).

Fig. 21 plots the time history of the mean-square displacement, $\langle r^2(t) \rangle$, of cellphone users in the greater Jacksonville area shown in Fig. 7 that were recorded during the period August 1, to November 30, 2017, and appeared close to the top of the hour at least $P = 540$ times during the entire duration of each month. Fig. 22 compares the recorded MSD $= \langle r^2(t) \rangle$ of the citizens of the greater Jacksonville area during the period August 1, to November 30, 2017, shown in Fig. 21 with the predictions of the calibrated amplitude-modulation model given by Eqs. (6) or (9) under normal steady-state operational conditions (No event) with $A_0 = 100\ \mathrm{km}^2$, $C = 0.6$, and $\gamma = 0.25$.

Again, in accordance with what has been calculated for the cities of Houston and Miami, the mean values of the Jacksonville MSD $= 100\ \mathrm{km}^2$ for year 2017 is larger than the mean value of the Jacksonville MSD $= 90\ \mathrm{km}^2$ for year 2021 due to the changes in the commuting patterns of the citizens during the postpandemic era.

Fig. 23 plots for the greater Jacksonville area the corresponding plots appearing in Fig. 17 that were analyzed in detail for the city of Houston when hit by Hurricane Harvey and reveal once again that

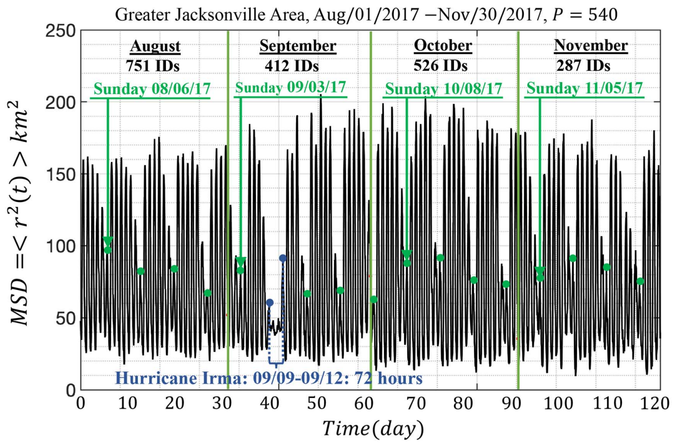

Fig. 21. Time history of the mean-square displacement $= \langle r^2(t) \rangle$ (ensemble average) of cellphone IDs in the greater Jacksonville that which appeared at least $P = 540$ times per month during the period August 1, to November 30, 2017. Dots atop the suppressed spikes indicate Sundays.

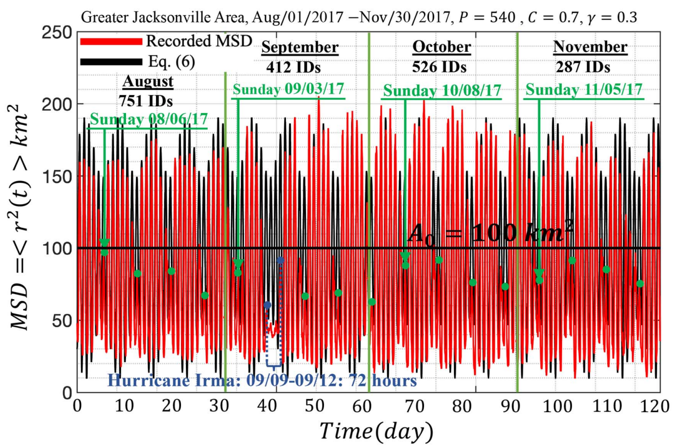

Fig. 22. Comparison of the predictions of the amplitude-modulation model ($A_0 = 100\ \mathrm{km}^2$, $C = 0.6$, and $\gamma = 0.25$) given by Eq. (6) under normal steady-state operational conditions (no event) in the greater Jacksonville area with the recorded mean-square displacement $\langle r^2(t) \rangle$ of the distilled number of IDs shown in the figure for each month during the period August 1, to November 30, 2017.

our analytical model expressed with Eqs. (6) or (9) captures the recorded posthurricane response of the city of Jacksonville with remarkable accuracy as shown in Fig. 23(d). Synchronization of the recorded and predicted postevent MSDs is achieved by selecting a pulse period $T_e = 3\text{days} = 72$ h; therefore, the greater Jacksonville area revert immediately to its prehurricane steady-state regime.

The September 2019 Hurricane Dorian

Hurricane Dorian was an extremely powerful category 5 Atlantic hurricane that is recorded as the most intense tropical cyclone to strike the Bahamas. A weakened category 2 storm, Dorian passed Northeast Florida nearly 90 miles offshore in the Atlantic Ocean. The storm left ports of St. Agustin and flood-prone area in Jacksonville inundated; yet, officially did not receive reports of major

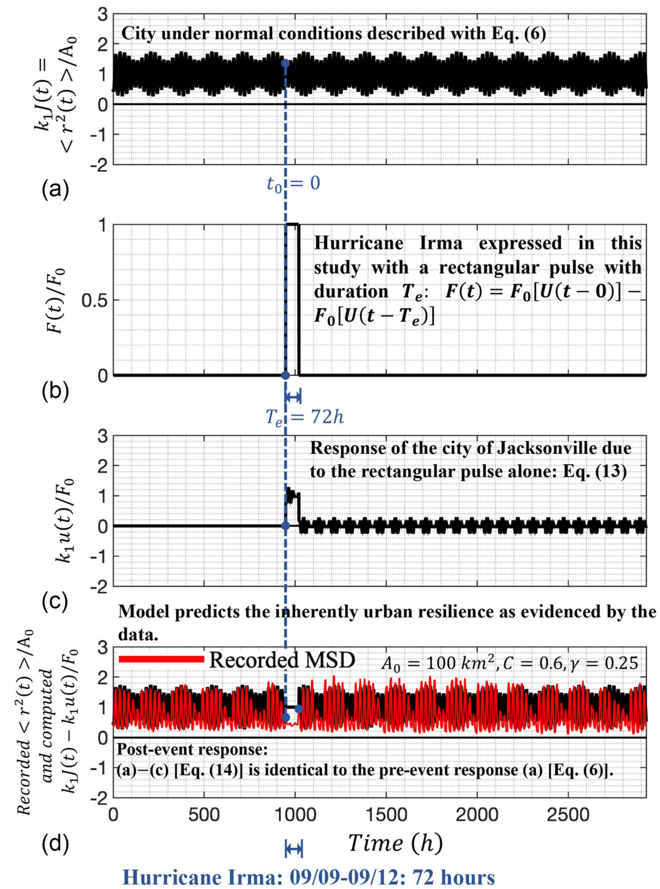

Fig. 23. (a) Normalized behavior of the city of Jacksonville under normal conditions as given by Eq. (6); (b) Acute shock on a city expressed with a rectangular pulse with a duration $T_e = 72$ h that is not an integer multiple of a day $= 24$ h; (c) Normalized response of the city of Jacksonville to the rectangular pulse alone with duration $T_e = 72$ h; and (d) Preevent and postevent response of Jacksonville [(a–c), solid dark lines] that is identical to the preevent response of the city (a). The thin red lines are the normalized MSD of the Jacksonville metroplex prior to, during, and after Hurricane Irma that happened in September 2017 as distilled from the recorded GPS location data.

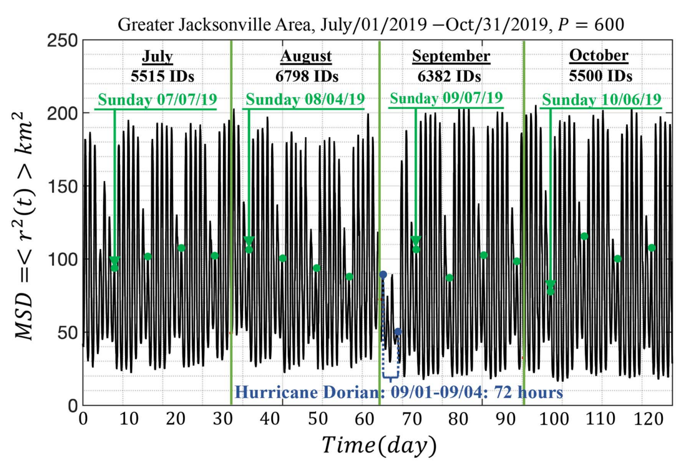

Fig. 24. Time history of the mean-square displacement $= \langle r^2(t) \rangle$ (ensemble average) of cellphone IDs in the greater Jacksonville area which appeared at least $P = 600$ times per month during the period July 1, to October 31, 2019. Dots atop the suppressed spikes indicate Sundays.

J. Eng. Mech., 2023, 149(10): 04023076

flooding. The city of Jacksonville, Florida, announced mandatory evacuations effective on Monday morning September 2, 2019.

Fig. 24 plots the time history of the mean-square displacement $\langle r^2(t)\rangle$, of the cellphone users in the greater Jacksonville area shown in Fig. 7 that were recorded during the period July 1, to October 31, 2019, and appeared close to the top of the hour at least $P = 600$ times during the entire duration of each month. The recorded MSD shows clearly that on Monday, September 02, 2019, the citizens of the greater Jacksonville area are following the evacuation orders and they returned by Thursday, September 5, 2019, following a tropical storm on Wednesday, September 4 (Mazzei and Bogel-Burroughs 2019). The city of Jacksonville resumes a normal operating regime by late Thursday, September 5, 2019.

Conclusions

This paper contributes to emerging trends for developing a quantitative, predictive framework for quantifying urban resilience. Our study concentrates on a "single-state equilibrium" that is the response history of the mean-square displacement of the citizens of the entire city when it operates under normal conditions and proceeds by examining the recorded mean-square displacement $\langle r^2(t)\rangle = \mathrm{MSD}$ of thousands of cellphone IDs from (1) three large US cities (Houston, Miami, and Jacksonville) when struck by category 4 and 5 hurricanes (2017 Harvey, 2017 Irma, and 2019 Dorian), and (2) the metroplexes of Dallas and Houston that were subjected to the February 2021 North American winter storm.

Our study shows that following any natural hazard, the recorded postevent MSD resumes its preevent regime within a very short time ranging from immediately up to 24 h after the end of the intense hazard, indicating that large American cities exhibit an inherent resilience to natural hazards within the context of engineering resilience (Holling 1996). The analysis presented in this paper is system wide for the entire urban center. A future study will focus on quantifying: (1) the recovery time of smaller, local communities in these large American cities when struck by natural hazards, and (2) the recovery time of other cities around the world with different resources and socioeconomic structures.

Our study also employs a previously developed mechanical model for large cities that was derived by the authors by making the conjecture that the $\mathrm{MSD} = \langle r^2(t)\rangle$ of cities is proportional to the creep compliance of the proposed model (Makris et al. 2023). This conjecture is rooted in Langevin dynamics which offers remarkable predictions for the macroscopic frequency and time-response functions of complex viscoelastic materials by only monitoring the thermally driven Brownian motion of probe microparticles immersed within the viscoelastic material. Our mechanical model for large cities predicts precisely what is uncovered by the data—that following the natural hazard, large cities revert to their initial steady-state behavior and resume their normal preevent activities. Accordingly, our study presented both an inductive and a deductive route for quantifying urban resilience. The inductive route (a pattern recognition route that can be falsified with a counterexample) concludes inherent urban resilience by merely observing the recovery of the recorded MSDs of the aforementioned cities when struck by historic hurricanes and winter storms. The deductive route that is central in our study hinges on the premise that the MSD of a city is proportional to the creep compliance of a mechanical model (in accordance with what emerges from quantitative Brownian motion and Langevin dynamics), and upon the premise is validated (from the aforementioned case studies), a quantitative analysis framework emerges with predictive capabilities.

Data Availability Statement

All data, models, or code that support the findings of this study are available from the corresponding author upon reasonable request.

Acknowledgments

This work was funded by the SMU/Bush Institute postdoctoral program and by the SMU-Lyle interdisciplinary seed funding initiative with No. 20-43-0061-S320086. Data analysis was performed on the ManeFrame II (M2): high-performance computing (HPC) cluster supported by SMU Research and Data Science Services.

References

Amadeo, K. 2018. "Hurricane Harvey facts, damage and costs." Accessed January 20, 2019. https://www.lamar.edu/_files/documents/resilience-recovery/grant/recovery-and-resiliency/hurric2.pdf.

Attard, P. 2012. *Non-equilibrium thermodynamics and statistical mechanics: Foundations and applications*. Oxford, UK: OUP Oxford.

Bettencourt, L., and G. West. 2010. "A unified theory of urban living." *Nature* 467 (7318): 912–913. https://doi.org/10.1038/467912a.

Bettencourt, L. M. 2013. "The origins of scaling in cities." *Science* 340 (6139): 1438–1441. https://doi.org/10.1126/science.1235823.

Bettencourt, L. M., and J. Kaur. 2011. "Evolution and structure of sustainability science." *PNAS* 108 (49): 19540–19545. https://doi.org/10.1073/pnas.1102712108.

Boussinesq, J. 1885. "Sur la resistance qu'oppose un fluide indefini en repos, sans pesanteur, au mouvement varie d'une sphere solide qu'il mouille sur toute sa surface, quand les vitesses restent bien continues et assez faibles pour que leurs carres et produits soient negligiables." *CR Acad. Sci.* 100: 935–937.

Brockerhoff, M. 1998. "World urbanization prospects: The 1996 revision." *Popul. Dev. Rev.* 24 (4): 883–885. https://doi.org/10.2307/2808041.

Bruneau, M., S. E. Chang, R. T. Eguchi, G. C. Lee, T. D. O'Rourke, A. M. Reinhorn, M. Shinozuka, K. Tierney, W. A. Wallace, and D. VonWinterfeldt. 2003. "A framework to quantitatively assess and enhance the seismic resilience of communities." *Earthquake Spectra* 19 (4): 733–752. https://doi.org/10.1193/1.1623497.

Cimellaro, G. P., A. M. Reinhorn, and M. Bruneau. 2010. "Framework for analytical quantification of disaster resilience." *Eng. Struct.* 32 (11): 3639–3649. https://doi.org/10.1016/j.engstruct.2010.08.008.

Clough, R., and J. Penzien. 1970. *Dynamics of structures*. New York: McGraw-Hill.

Coffey, W., and Y. P. Kalmykov. 2012. *The Langevin equation: With applications to stochastic problems in physics, chemistry and electrical engineering*. Hackensack, NJ: World Scientific Publishing.

Cruz, S. S., J. P. T. Costa, S. Á. D. Sousa, and P. Pinho. 2013. "Urban resilience and spatial dynamics." In *Proc., Resilience Thinking in Urban Planning*, 53–69. New York: Springer.

Da Silva, J., S. Kernaghan, and A. Luque. 2012. "A systems approach to meeting the challenges of urban climate change." *J. Urban Sustainable Dev.* 4 (2): 125–145. https://doi.org/10.1080/19463138.2012.718279.

Ehlinger, S. 2017. "Hurricane Harvey leaves Texans without internet, phone service." Accessed August. 28, 2017. https://www.mysanantonio.com/business/technology/article/Hurricane-Harvey-leaves-Texans-without-internet-12069233.php.

Einstein, A. 1905. "Über die von der molekularkinetischen theorie der wärme geforderte bewe gung von in ruhenden flüssigkeiten suspendierten teilchen." *Ann. Phys.* 322: 549–560.

Gao, J., S. V. Buldyrev, H. E. Stanley, and S. Havlin. 2012. "Networks formed from interdepend dent networks." *Nature Phys.* 8 (1): 40–48. https://doi.org/10.1038/nphys2180.

Gittes, F., B. Schnurr, P. Olmsted, F. C. MacKintosh, and C. F. Schmidt. 1997. "Microscopic viscoelasticity: Shear moduli of soft materials determined from thermal fluctuations." *Phys. Rev. Lett.* 79 (17): 3286. https://doi.org/10.1103/PhysRevLett.79.3286.

Godschalk, D. R. 2003. “Urban hazard mitigation: Creating resilient cities.” *Nat. Hazards Rev.* 4 (3): 136–143. https://doi.org/10.1061/(ASCE)1527-6988(2003)4:3(136).

Gray, L., and R. Graham. 1961. *Radio transmitters*. New York: McGraw-Hill.

Harris, C. M., and C. B. Crede. 1976. *Shock and vibration handbook*. New York: McGraw-Hill.

Holling, C. S. 1973. “Resilience and stability of ecological systems.” *Annu. Rev. Ecol. Evol. Syst.* 4 (1): 1–23. https://doi.org/10.1146/annurev.es.04.110173.000245.

Holling, C. S. 1996. “Engineering resilience versus ecological resilience.” *Eng. Ecol. Constraints* 31 (Apr): 32.

Huang, R., I. Chavez, K. M. Taute, B. Lukić, S. Jeney, M. G. Raizen, and E.-L. Florin. 2011. “Direct observation of the full transition from ballistic to diffusive Brownian motion in a liquid.” *Nat. Phys.* 7 (7): 576–580. https://doi.org/10.1038/nphys1953.

Huber, C. 2018. “World vision, 2017 Hurricane Irma: Facts, FAQs, and how to help.” Accessed September 8, 2017. https://www.worldvision.org/disaster-relief-news-stories/2017-hurricane-irma-facts.

Jabareen, Y. 2013. “Planning the resilient city: Concepts and strategies for coping with climate change and environmental risk.” *Cities* 31 (Apr): 220–229. https://doi.org/10.1016/j.cities.2012.05.004.

Jannasch, A., M. Mahamdeh, and E. Schäffer. 2011. “Inertial effects of a small Brownian particle cause a colored power spectral density of thermal noise.” *Phys. Rev. Lett.* 107 (22): 228301. https://doi.org/10.1103/PhysRevLett.107.228301.

Landau, L. D., and E. M. Lifshitz. 1959. *Fluid mechanics: Course of theoretical physics*. Oxford, UK: Pergamon Press.

Landau, L. D., and E. M. Lifshitz. 1980. “Statistical *physics*.” In Vol. 5 of *Course of theoretical physics*. Amsterdam, Netherlands: Elsevier.

Langevin, P. 1908. “Sur la théorie du mouvement Brownian.” *C. R.* 146 (Mar): 530–533.

Lhomme, S., D. Serre, Y. Diab, and R. Laganier. 2013. “Urban technical networks resilience assessment.” *Resilience Urban Risk Manage.* 109–117.

Li, T., and M. G. Raizen. 2013. “Brownian motion at short time scales.” *Ann. Phys.* 525 (4): 281–295. https://doi.org/10.1002/andp.201200232.

Lighthill, M. J. 1958. *An introduction to Fourier analysis and generalised functions*. Cambridge, UK: Cambridge University Press.

Makris, N. 2017. “Basic response functions of simple inertoelastic and inertoviscous models.” *J. Eng. Mech.* 143 (11): 04017123. https://doi.org/10.1061/(ASCE)EM.1943-7889.0001348.

Makris, N. 2018. “Time-response functions of mechanical networks with inerters and causality.” *Meccanica* 53 (9): 2237–2255. https://doi.org/10.1007/s11012-018-0822-6.

Makris, N. 2020. “Viscous-viscoelastic correspondence principle for Brownian motion.” *Phys. Rev. E* 101 (5): 052139. https://doi.org/10.1103/PhysRevE.101.052139.

Makris, N. 2021a. “Impulse response function for Brownian motion.” *Soft Matter* 17 (21): 5410–5426. https://doi.org/10.1039/D1SM00380A.

Makris, N. 2021b. “A rheological analog for Brownian motion with hydrodynamic memory.” *Phys. Fluids* 33 (7): 072014. https://doi.org/10.1063/5.0059452.

Makris, N., G. Moghimi, E. Godat, and T. Vu. 2023. “Mechanical analogue for cities.” *R. Soc. Open Sci.* 10 (3): 220943. https://doi.org/10.1098/rsos.220943.

Mason, T. G. 2000. “Estimating the viscoelastic moduli of complex fluids using the generalized Stokes–Einstein equation.” *Rheol. Acta* 39 (4): 371–378. https://doi.org/10.1007/s003970000094.

Mason, T. G., K. Ganesan, J. H. van Zanten, D. Wirtz, and S. C. Kuo. 1997a. “Particle tracking microrheology of complex fluids.” *Phys. Rev. Lett.* 79 (17): 3282. https://doi.org/10.1103/PhysRevLett.79.3282.

Mason, T. G., H. Gang, and D. A. Weitz. 1997b. “Diffusing-wave-spectroscopy measurements of viscoelasticity of complex fluids.” *JOSA A* 14 (1): 139–149. https://doi.org/10.1364/JOSAA.14.000139.

Mason, T. G., and D. A. Weitz. 1995. “Optical measurements of frequency-dependent linear viscoelastic moduli of complex fluids.” *Phys. Rev. Lett.* 74 (7): 1250. https://doi.org/10.1103/PhysRevLett.74.1250.

Mazzei, P., and N. Bogel-Burroughs. 2019. “The New York Times.” Accessed September 6, 2019. https://www.nytimes.com/2019/09/04/us/hurricane-dorian-updates.html.

Meerow, S., J. P. Newell, and M. Stults. 2016. “Defining urban resilience: A review.” *Landscape Urban Plann.* 147 (Mar): 38–49. https://doi.org/10.1016/j.landurbplan.2015.11.011.

National Weather Service. 2021. “North American winter storm in Dallas.” Accessed February 21, 2021. https://www.weather.gov/fwd/Feb-2021-WinterEvent.

NOAA (National Oceanic and Atmospheric Administration). 2021. “North American winter storm in Dallas.” Accessed March 8, 2021. https://www.noaa.gov/news/us-had-its-coldest-february-in-more-than-30-years.

Oppenheim, A. V., and R. W. Schafer. 1975. *Digital signal processing*. Englewood Cliffs, NJ: Prentice-Hall.

Ornstein, L. S. 1917. “On the Brownian motion.” In Vol. 21 of *Proc., Huygens Institute-Royal Netherlands Academy of Arts and Sciences*, 96–108. Amsterdam, Netherlands: Huygens Institute for the History of the Netherlands.

Reid, J. G. 1983. *Linear system fundamentals: Continuous and discrete, classic and modern*. New York: McGraw-Hill Science, Engineering & Mathematics.

Schnurr, B., F. Gittes, F. MacKintosh, and C. Schmidt. 1997. “Determining microscopic viscoelasticity in flexible and semiflexible polymer networks from thermal fluctuations.” *Macromolecules* 30 (25): 7781–7792. https://doi.org/10.1021/ma970555n.

Silver, H. W. 2011. *The ARRL handbook: For radio communications*. Newington, CT: Amer Radio Relay League.

Smith, A. B., and R. W. Katz. 2013. “US billion-dollar weather and climate disasters: Data sources, trends, accuracy and biases.” *Nat. Hazards* 67 (2): 387–410. https://doi.org/10.1007/s11069-013-0566-5.

Stepzinski, T. 2017. “The Florida Times-Union.” Accessed September 18, 2017. https://web.archive.org/web/20180125080131/http://jacksonville.com/news/metro/clay/2017-09-18/storm-surge-damage-hurricane-irma-forces-orange-park-condo-owners-homes.

Tropical Winds Newsletter. 2017. “Tropical Winds Newsletter (report).” National Weather Service. Accessed September 20, 2017. https://www.weather.gov/.

Uhlenbeck, G. E., and L. S. Ornstein. 1930. “On the theory of the Brownian motion.” *Phys. Rev.* 36 (5): 823. https://doi.org/10.1103/PhysRev.36.823.

Vu, T. M., and A. K. Mishra. 2019. “Nonstationary frequency analysis of the recent extreme precipitation events in the United States.” *J. Hydrol.* 575 (Aug): 999–1010. https://doi.org/10.1016/j.jhydrol.2019.05.090.

Wang, M. C., and G. E. Uhlenbeck. 1945. “On the theory of the Brownian motion II.” *Rev. Mod. Phys.* 17 (2–3): 323. https://doi.org/10.1103/RevModPhys.17.323.